

TOPICAL REVIEW






# Electron transport in biomolecular gaseous and liquid systems: theory, experiment and self-consistent cross-sections

To cite this article: R D White *et al* 2018 *Plasma Sources Sci. Technol.* **27** 053001

View the [article online](#) for updates and enhancements.

## Topical Review

# Electron transport in biomolecular gaseous and liquid systems: theory, experiment and self-consistent cross-sections

R D White<sup>1</sup> , D Cocks<sup>1,2</sup> , G Boyle<sup>1</sup>, M Casey<sup>1</sup>, N Garland<sup>1</sup> ,  
D Konovalov<sup>1</sup>, B Philippa<sup>1</sup>, P Stokes<sup>1</sup>, J de Urquijo<sup>3</sup>, O González-Magaña<sup>3</sup>,  
R P McEachran<sup>2</sup>, S J Buckman<sup>2</sup>, M J Brunger<sup>4</sup> , G Garcia<sup>5</sup>, S Dujko<sup>6</sup> and  
Z Lj Petrovic<sup>6</sup> 

<sup>1</sup> College of Science and Engineering, James Cook University, Townsville, QLD, Australia

<sup>2</sup> Research School of Physics and Engineering, ANU, Canberra, ACT, Australia

<sup>3</sup> Instituto de Ciencias Físicas, Universidad Nacional Autónoma de México, Cuernavaca, México

<sup>4</sup> College of Science and Engineering, Flinders University, Adelaide, SA, Australia

<sup>5</sup> Instituto de Física Fundamental, Consejo Superior de Investigaciones Científicas (CSIC), Madrid, Spain

<sup>6</sup> Institute of Physics, University of Belgrade, Zemun, Belgrade, Serbia

E-mail: [ronald.white@jcu.edu.au](mailto:ronald.white@jcu.edu.au)

Received 16 November 2017, revised 26 February 2018

Accepted for publication 12 April 2018

Published 15 May 2018



CrossMark

## Abstract

Accurate modelling of electron transport in plasmas, plasma-liquid and plasma-tissue interactions requires (i) the existence of accurate and complete sets of cross-sections, and (ii) an accurate treatment of electron transport in these gaseous and soft-condensed phases. In this study we present progress towards the provision of self-consistent electron-biomolecule cross-section sets representative of tissue, including water and THF, by comparison of calculated transport coefficients with those measured using a pulsed-Townsend swarm experiment. Water–argon mixtures are used to assess the self-consistency of the electron-water vapour cross-section set proposed in de Urquijo *et al* (2014 *J. Chem. Phys.* **141** 014308). Modelling of electron transport in liquids and soft-condensed matter is considered through appropriate generalisations of Boltzmann's equation to account for spatial-temporal correlations and screening of the electron potential. The *ab initio* formalism is applied to electron transport in atomic liquids and compared with available experimental swarm data for these noble liquids. Issues on the applicability of the *ab initio* formalism for krypton are discussed and addressed through consideration of the background energy of the electron in liquid krypton. The presence of self-trapping (into bubble/cluster states/solvation) in some liquids requires a reformulation of the governing Boltzmann equation to account for the combined localised–delocalised nature of the resulting electron transport. A generalised Boltzmann equation is presented which is highlighted to produce dispersive transport observed in some liquid systems.

Keywords: plasmas, liquids, biomolecules, Boltzmann equation, electron swarms, transport coefficients

## 1. Introduction

The application of plasmas in medicine is a key new field that relies on the synergistic effects of plasmas interacting with

human tissue and liquids (see the roadmaps [1–3]). Optimization of efficacy and selectivity of future generation plasma-medicine is dependent on (among other things) a detailed understanding of the underlying fundamental microscopic

physics and associated predictive modelling. Electron-induced processes and interactions with biomolecules that constitute human tissue (e.g. water, DNA bases and sugars) play a key, though understudied, role in these systems [1–3], and there remain many fundamental research questions that underpin this understanding.

As a necessary input, progress in plasma-based medical applications requires a comprehensive database of electron-induced processes in representative biomolecules so that informed predictive models including electron transport in human tissue can be constructed. The atomic and molecular physics community has been active in this space, both theoretically and experimentally, and there are a number of biologically relevant targets for which electron scattering cross-sections have been extensively studied. Of particular note is water: as the natural surrogate for human tissue it has received particular attention [4–16]. More recently, while electron scattering from DNA is currently not convenient to study, electron scattering from tetrahydrofuran (THF–C<sub>4</sub>H<sub>8</sub>O) has been systematically investigated as a close analogue for 2-deoxyribose, a sugar that links phosphate groups in the DNA backbone [17–25]. Electron scattering from other biologically relevant molecules studied include pyrimidine, tetrahydrofurfuryl alcohol, para-benzoquinone and others [23, 26–31], and the reader is referred to the comprehensive review a10.1088 [32] for further details.

Despite the wealth of scattering information for electron-biomolecule interactions, there are always issues associated with the completeness and accuracy of the electron-biomolecule cross-section sets subsequently formed. In recent times we have developed a programme for the measurement, assessment and subsequent application of electron interactions with biologically relevant molecules [8, 12, 13, 17, 18, 24]. Our rationale is to establish the most accurate cross-sections for all relevant collision processes, by combining accurate measurement of scattering events with contemporary, state-of-the-art molecular theoretical models. These cross-sections are compiled into self-consistent sets, which are then tested for accuracy and completeness using the swarm process [33–36]. In a swarm experiment, electrons are driven through a gas (or liquid) under the influence of an electric (and possibly magnetic) field and the associated currents are measured and interpreted in terms of transport coefficients. The electron velocity distributions are distinctly non-equilibrium and this non-equilibrium nature varies as the applied field to pressure ratio is varied. Comparison of calculated and measured swarm transport properties provides an assessment of the pa10.1088, momentum and energy balance within the cross-section set. Iterative adjustments within the error bars of the experiment and theory can then yield cross-section sets with a measure on the self-consistency of the electron-biomolecule cross-section set [8, 12, 13, 15, 19, 37, 38].

The transition from the gas phase to address electron transport in biological soft-condensed matter for modelling plasma-tissue interactions is an extremely difficult problem. The crudest approximation is to scale the dilute gas phase results to liquid densities. Experimental evidence however

indicates that the treatment of electron transport in the liquid-phase is considerably more complex than this—even for simple atomic liquids and particularly at low-energies [39–47]. We have developed a programme that aims to address those deficiencies. Our starting point has been to consider electron transport in cryogenic atomic liquids as the simplest prototype of electron transport in liquids. For such systems there exists a wealth of electron swarm experiments [39, 41–50] to facilitate benchmarking of the theoretical foundations.

There are various theoretical approaches to the modelling of electron transport in atomic liquids [39–43, 45, 46, 48–53]. Generally these theories have restricted domains of validity and are separated into various models dependent on the inherent mobility of electrons within the dielectric liquid. For high-mobility liquids (e.g. argon, xenon, krypton) the electron is treated essentially as a ‘free’ pa10.1088 that is coherently scattered from atoms/molecules in the background medium which exhibits short range order but no/limited long-range order of atoms/molecules which are in thermal motion. Scattering is treated through an effective single pa10.1088 scattering process, where the dominant effects that are included in its calculation are (i) the liquid structure and the spatial and temporal correlations of the constituent molecules within the soft-matter, (ii) the modifications to the electron interaction potential within the liquid environment, and (iii) the background energy of the electron within the liquid or equivalently the energy at the bottom of the conduction band,  $V_0$  [39–43, 46, 48–51].

While the foundations for accounting for the liquid’s temporal and spatial correlations are clear [51], there exists a variety of different methods for calculating the effective scattering potential that the electron sees within the liquid [39–43, 48–50]. The foundations were laid by Lekner [40], building up the effective potential from the electron-single atom potential and the pair correlation function. Atrazhev and co-workers [54, 55] simplified this process by identifying that the cross-section at low-energies became energy independent and dependent solely on density. The energy range for constancy in the cross-section was a flexible parameter that was empirically determined. In subsequent studies, Atrazhev and co-workers [49, 50, 56] developed a theory for calculating the cross-section based on a muffin tin potential using a variable phase-function method with an effective range defined by the Wigner–Seitz sphere surrounding each atom in the liquid. The quantity  $V_0$  has been addressed using different approaches, including an assumption of quasi-periodicity inside of Wigner–Seitz cells [57–60], extensions to include perturbations due to the distribution of atomic positions [61] and path-integral techniques [62, 63]. More recently, Evans and co-workers have proposed a local-Wigner–Seitz theory to calculate  $V_0$ . They combine these calculations with field enhanced photoemission [64] and field-ionisation measurements [65] to obtain  $V_0$  in a variety of gases and liquids, and explore parameter regimes that include the critical point in these species.

In contrast to the above, a number of other theories emerged whose foundations are different. Sakai *et al* [42, 43] used a swarm-derived iterative fitting procedure to adjust the momentum transfer cross-sections (and an inelastic process) to fit the experimental transport data. Borghesani and co-workers [46] heuristically combined the liquid effects identified above to obtain an effective cross-section, utilising gas phase cross-sections and sampling shifted energies to account for the  $V_0$  effects. Their results continue to be very accurate and could predict the enhancements/reductions in the zero-field mobility. Likewise, the theory developed by Braglia and Dallacasa [66] using a Green's function approach with appropriate approximations to the self-energy could explain this behaviour. Unfortunately they did not go beyond linear response theory and hence their theory was not able explain non-equilibrium behaviour at high fields.

For low electron mobility liquids (e.g. neon, hydrogen, water, etc), the physical mechanisms present for electrons are distinctly different. Polischuk [67, 68] applied the Green's function approach to calculate mobility in dense polar gases from the vertex functions, accounting for the anisotropic nature of the scatterers, comparing to the measurements and theory of Krebs and co-workers [69–71]. In addition to the above scattering processes, in such systems electrons can be trapped (self-trapped) within the liquid through a variety of different mechanisms [61, 72–79] and the electron becomes localised in space. Some trapped states can be quite stable while others may only be weakly bound [41, 61, 72, 73]. The transport is thus physically both localised and delocalised in nature. Gallicchio and Berne [80] obtained real-time correlators by maximum entropy inverse of imaginary-time path-integral Monte Carlo calculations. This allowed them to extract both the existence of localised states and the diffusion coefficient of delocalised states. There were attempts to theoretically model this transport behaviour [41, 45], however there was no unified model developed to describe the non-equilibrium behaviour observed for neon.

Recently, we have attempted to develop an *ab initio* unified theory, which builds upon the foundational works [39–43, 45, 46, 48–51] accounting for the various components associated with scattering detailed above [81, 82], as well as the combined localised–delocalised nature of transport that has been demonstrated to exist in such media [41, 83]. We bring to bear the modern day scattering and transport theory, overcoming a number of approximations that are present in some of the earlier investigations. We avoid the use of approximate potentials (e.g. the Buckingham potential which neglects the exchange interaction—the errors of which we have highlighted previously [81], or the retention of only the important parts of the potentials [49]), and instead use the accurate forms for the electron–atom interaction which are systematically benchmarked in the gas phase. From a transport theory viewpoint, we develop and implement a multi-term Boltzmann equation solution framework to model highly non-equilibrium electron transport in liquids. All previous

theories have been two-term in nature, which *a priori* assumes a quasi-isotropic velocity distribution and restricts the ability to account for the highly anisotropic nature of the effective differential scattering cross-section for electrons in liquids.

We begin this study in section 2 with a brief review of Boltzmann's equation and the associated multi-term solution technique. In section 3, we present results for both gaseous water and THF, including new self-consistency checks of the water cross-sections through an analysis of mixtures with argon gas. The foundations for our *ab initio* treatment for electrons in atomic liquids are detailed in section 4, and applied to the development of scattering cross-sections for electrons in liquid argon and liquid krypton. The self-consistency of these cross-sections is assessed through comparison with available swarm experiments in the associated liquids. In section 5, we consider evidence for other physical processes present in liquids and highlight further and future modifications to transport theories required to treat electron transport in general liquid and soft-condensed systems. We conclude in section 6 with a summary, together with some key challenges for further studies in this domain.

## 2. Theory

### 2.1. Multi-term solution of Boltzmann's equation

Non-equilibrium electrons drifting and diffusing through matter, whether it be in the gaseous, liquid or a soft-condensed state, subject to an external electric field  $\mathbf{E}$ ; can be described by the solution of Boltzmann's equation for the phase-space distribution function  $F(\mathbf{r}, \mathbf{v}, t)$ :

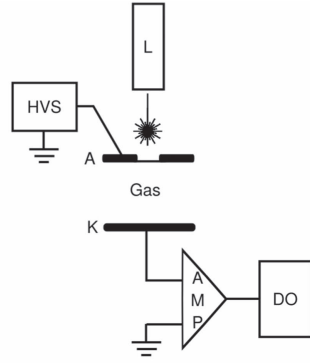
$$\frac{\partial F}{\partial t} + \mathbf{v} \cdot \nabla F + \frac{e\mathbf{E}}{m_e} \cdot \frac{\partial F}{\partial \mathbf{v}} = -J(F), \quad (1)$$

where  $\mathbf{r}$ ,  $\mathbf{v}$  and  $e$  denote the position, velocity and charge of the electron respectively. The collision operator  $J(f)$  accounts for all the necessary collision types and interactions between the electrons of mass  $m_e$  and the background medium. For each process in each mixture component, there are various contributions to the collision operator associated with the various collision processes:

$$J(F, F_0) = \sum_i \alpha_i [J_{WUB}(F, F_0^i) + J_A(F, F_0^i) + J_I(F, F_0^i) + \dots], \quad (2)$$

where the sum is over the components in the mixture,  $\alpha_i$  represents the mole fraction of component  $i$  and  $F_0^i$  is its neutral velocity distribution function. Suppressing the mixture index, the elastic, inelastic and super elastic collisions in the gas phase are described by [84]:

$$J_{WUB}(F, F_0) = \sum_{jk} \int [F(\mathbf{r}, \mathbf{v}, t) F_{0j}(\mathbf{v}_0) - F(\mathbf{r}, \mathbf{v}', t) F_{0k}(\mathbf{v}_0')] g \sigma(jk; g \chi) d\hat{\mathbf{g}}' d\mathbf{v}_0 \quad (3)$$



L: UV pulsed laser  
 HVS: High voltage supply  
 AMP: Amplifier  
 DO: Digital oscilloscope

**Figure 1.** Schematic representation of the pulsed-Townsend experiment. A denotes the anode while K denotes the cathode. Note that the central region of the anode is a planar copper mesh (2.8 lines/mm) through which the laser passes to strike the cathode.

and  $\sigma(jk; g\chi)$  is the differential cross-section for the scattering process  $(j, \mathbf{v}, \mathbf{v}_0) \rightarrow (k, \mathbf{v}', \mathbf{v}'_0)$ ; with  $\cos \chi = \mathbf{g} \cdot \mathbf{g}'$  where  $\mathbf{g}$  represents the relative velocity in the collision, and  $j, k$  are the internal states of the molecule.  $F_{0j}(\mathbf{v}_0)$  is a Maxwell–Boltzmann distribution for neutrals with internal state  $j$ . Electron attachment processes (e.g. dissociative electron attachment (DEA)) are described by:

$$J_A(F, F_0) = \sum_j F(\mathbf{r}, \mathbf{v}, t) \int F_{0j}(\mathbf{v}_0) g \sigma_A(j; g) d\mathbf{v}_0, \quad (4)$$

where  $\sigma_A(j, g)$  is the relevant attachment cross-section. The ionisation operator implemented takes the form [85]:

$$J_I(F, F_0) = \sum_j n_{0j} \{ \nu \sigma_I(j; \nu) F(\mathbf{r}, \mathbf{v}, t) \}, \\ - 2 \int \nu' \sigma_I(j; \nu') B(\mathbf{v}, \mathbf{v}'; j) F(\mathbf{r}, \mathbf{v}', t) d\nu', \quad (5)$$

where  $\sigma_I(j, \nu)$  is the ionization cross-section and  $B(\mathbf{v}, \mathbf{v}'; j)$  is the probability for one of the two electrons after ionisation having a velocity in the range of  $\nu$  to  $\nu + d\nu$ ; for incident electron velocity  $\nu'$ .

Modifications to the collision operators to account for additional processes present in soft-condensed matter (e.g. coherent scattering and the combined localised–delocalised nature) are detailed below in sections 4.1 and 5.

With all collision operators defined, the first step in solution of (1) is typically the representation of the distribution function in directions of velocity space through an expansion in spherical harmonics  $Y_m^{[l]}(\hat{\mathbf{v}})$ :

$$F(\mathbf{r}, \mathbf{v}, t) = \sum_{l=0}^{l_{\max}} \sum_{m_l=-l}^l f_m^{(l)}(\mathbf{r}, \nu, t) Y_{m_l}^{[l]}(\hat{\mathbf{v}}), \quad (6)$$

where  $\hat{\mathbf{v}}$  denotes the angles of  $\mathbf{v}$ . Note that this reduces to an expansion in terms of Legendre polynomials  $P_l(\cos \theta)$  for the

rotational symmetry considered here. It has long been established that a *multi-term analysis* is often required, in which  $l_{\max}$  must be varied incrementally until some convergence/accuracy criterion is attained. It is not at all unusual to require an  $l_{\max} > 5$  to have transport coefficients accurate to better than 1% for electrons in molecular systems. Note that one simply increments  $l_{\max}$  until (6) (or integrals involving it) converges to within the desired accuracy.

For the transport coefficients under consideration in this study, using the orthogonality of spherical harmonics, combining (1) and (6) leads to the following system of coupled equations for  $f_m^{(l)}$  under spatially homogeneous conditions:

$$J^l f_m^{(l)} - \frac{eE}{m} \left\{ \frac{l+1}{2l+3} \left[ \frac{d}{d\nu} + \frac{l+2}{\nu} \right] f_m^{(l+1)} \right. \\ \left. - \frac{l}{2l-1} \left[ \frac{d}{d\nu} - \frac{l-1}{\nu} \right] f_m^{(l-1)} \right\} = 0. \quad (7)$$

The transport coefficients can then be calculated directly from solution of the above system of equation (7). Of particular note here, we consider the flux drift velocity via:

$$W = \frac{4\pi}{3} \int_0^\infty \nu f_0^{(1)}(\nu) \nu^2 d\nu, \quad (8)$$

where the distribution function is normalised according to  $4\pi \int_0^\infty f_0^{(0)}(\nu) \nu^2 d\nu = 1$ . The reduced effective ionization coefficient is calculated via:

$$R/n_0 = 4\pi \int_0^\infty (\sigma_I - \sigma_A) f_0^{(0)}(\nu) \nu^2 d\nu, \quad (9)$$

where  $n_0$  is the neutral number density, which can be directly related to the first Townsend ionization coefficient  $\alpha$  [86]. In this study we also compute the characteristic energy (ratio of the transverse diffusion coefficient to the mobility,  $D_T/\mu$ , where  $\mu = W/E$ ) [33]. For further details on the multi-term solution of Boltzmann's equation and calculation of the various transport coefficients the reader is referred to [87–89].

### 3. Towards self-consistent electron-biomolecule cross-section sets

As detailed in section 1, swarm experiments provide one of the key discriminating tests on the accuracy and completeness of cross-section sets [33, 35, 36]. In swarm experiments, electrons are passed through matter of known temperature and pressure (density) under the influence of applied external fields. Currents are interpreted in terms of transport coefficients such as drift velocities, diffusion coefficients and ionization/attachment rates. In the gas phase, experiments are conducted over a range of applied electric fields and pressures. Comparison of measured transport coefficients with those calculated from transport theory/simulation enables one to assess the ability of the proposed cross-section set to accurately represent pa10.1088, momentum and energy (and higher-order) balance.

In the current programme on swarm transport in gaseous systems, we utilise a pulsed-Townsend (PT) experiment



swarm technique to measure drift velocities, diffusion coefficients and various rate coefficients [90–93]. The primary aim is to build and then assess the completeness and accuracy of various electron-biomolecule cross-section sets.

### 3.1. Experimental measurement of electron transport coefficients using the PT method

A schematic of the PT experiment is shown in figure 1. Electrons are generated from the aluminium cathode by the incidence of a UV pulsed-laser (355 nm, 3 ns duration, 1 Hz repetition rate). The electrons (and their subsequent ions generated) are accelerated through the parallel plate capacitor arrangement via an applied potential difference, and a balance is achieved between the energy input from the field and that dissipated in collisions. The displacement current in the external circuit is measured, with the faster component representing the electrons and the slower component representing the ions generated. The analysis of the electron component enables the determination of the electron drift velocity, the longitudinal diffusion coefficient and the effective ionization coefficient [90, 91].

All the measurements were carried out at room temperature (291–301 K) and were measured with a thermocouple probe to an accuracy of  $\pm 0.5$  K. Measurements were repeated at various pressures and fixed  $E/n_0$ , with the low-pressure limit determined by the minimum anode voltage required to avoid space-charge effects. Explicit details for the experimental parameters used for electrons in pure water are presented in [8], while those for pure THF are detailed in [19]. Water–Ar mixtures with 5%, 10%, 20% and 50% water were studied here. In order to avoid water saturation effects, all water partial pressures were kept below 16 Torr (saturation vapour pressure is close to 20 Torr at the room temperatures used in these experiments). High purity water (Sigma Aldrich) was used throughout, while the Ar gas sample was obtained from Praxair with a stated purity of 99.995%. Gas mixtures were prepared inside the experimental chamber using an absolute capacitive pressure transducer with an accuracy of 0.15%. A fixed gap distance of 31 mm was used, set with a micrometer to an accuracy of 0.025 mm. Base vacuum pressures of  $2 \times 10^{-6}$  Torr could be achieved, while the minimum water–Ar mixture pressure used was 1 Torr.

### 3.2. Electron swarms in pure water and pure THF gases

In figure 2, we present experimental results for the drift velocity for electrons in pure water and pure THF. We consider the density-reduced electric field ( $E/n_0$ ) range from 0.1 to 1000 Td ( $1 \text{ Td} = 10^{-21} \text{ V m}^2$ ) while the background gas mixture temperature is fixed between 293 and 300 K for all measurements. The drift velocities between the two biomolecules are both quantitatively and qualitatively different. At low fields, the electron drift in water is lower than THF, while the situation is reversed at higher electric fields. For electrons in water, at reduced fields below approximately 35 Td, the deviation from thermal equilibrium is suppressed due to the

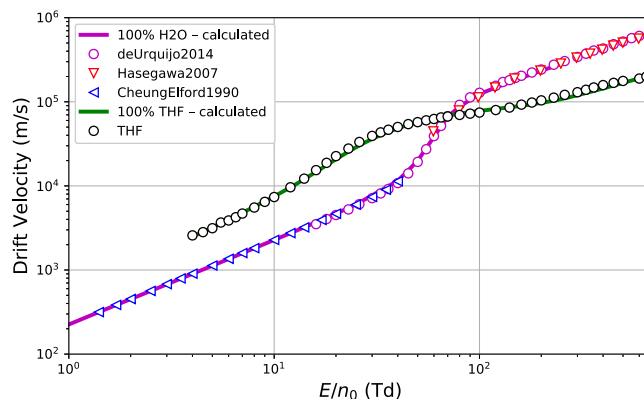


**Figure 2.** Comparison of the electron drift velocities in water vapour and THF. The water vapour results are calculated using the cross-section set proposed in [8] with the available experimental swarm measurements of Cheung and Elford [94], Hasegawa *et al* [9] and de Urquijo *et al* [8]. The THF results are calculated using the cross-section set proposed in [19] developed using the PT measurements in that same study.

the large number of rotational channels. For THF, the thermal equilibrium deadlock is broken at lower fields than for water, reflecting the reduced rotational cross-sections in THF. From 35 to 90 Td, a quasi-runaway situation develops for electrons in water vapour due to the rapidly falling momentum transfer and rotational cross-sections in this energy regime—the implications are discussed further below. For THF there is no such quasi-runaway regime. Above these fields, electronic and ionisation channels open up and the field variation of the drift velocity in both systems remain relatively constant between the two.

In the study of Ness *et al* [12] we revisited the issue of assessing the completeness, accuracy and consistency of electron-water vapour cross-section sets through comparisons of calculated transport coefficients with those measured in swarm experiments using an improved Boltzmann equation solution code to facilitate higher accuracy. That study focussed on sensitivity to the calculated transport coefficients arising from new cross-section measurements of the electronic-state excitations of Brunger and co-workers [14]. The cross-section set was refined in a subsequent study where mixtures of water vapour with helium were considered [8]. The primary modification was a slight change to the total momentum transfer cross-section which ensured self-consistency with the measured drift velocities in mixtures with helium to within approximately 5% over the range of reduced fields and He concentrations considered. The results for the pure water vapour are displayed in figure 2.

In the recent study of Casey *et al* [19], we revisited the set of cross-sections for electron impact on THF proposed by Garland *et al* [17] and utilised where appropriate new/updated cross-sections available since that study. Until the study of Casey *et al* [19] there was no experimental swarm data available to assess the self-consistency of the cross-section set proposed. A sensitivity study of the transport coefficients to the errors and uncertainties in the various

electron-THF scattering cross-sections was conducted. It was clear from the sensitivity study that there was physics missing from the available cross-sections. In addition to extrapolations to the existing elastic and DEA cross-sections where data/calculations did not exist, we found that additional energy deposition channels were required and which were proposed as neutral dissociation (ND) channels. ND cross-sections are not currently measurable and the swarm technique represents a possible means of establishing such cross-sections. Figure 2 demonstrates that the proposed cross-section set is essentially self-consistent with the available experimental swarm data. The reader is referred to [19] for further details.

### 3.3. Electron swarms in water–argon gas mixtures—a further assessment

A further test on the self-consistency of a particular cross-section set is to consider mixtures with an atomic/molecular species whose cross-sections are known accurately [34, 95–97]. This addition of the atomic/molecular species modifies the energy and momentum balance within the swarm, and consequently the velocity distribution of the electrons.

As detailed above, this process was adopted in [8], where the self-consistency of the water vapour cross-sections was assessed and improved using mixtures with helium. In this study, we present a further test on the self-consistency of electron-water cross-sections through the consideration of electrons in mixtures of water with argon. The electron impact cross-sections for argon are distinctly different to those in helium and hence the modifications to the energy distribution function arising over the reduced electric fields considered will sample the water vapour cross-sections in a manner different from those in the pure and helium mixture cases.

In figure 3, we present the experimental data for electrons in various water–argon mixture ratios ranging from 5% water to 50% water (see table A1 for tabulated values). It is clear that the drift velocity profiles are very sensitive to the mixture ratio, highlighting the modifications to the velocity distribution function. Interestingly, we observe for the 5% and 10% water mixture ratios the emergence of negative differential conductivity (NDC) [98, 99], i.e. the fall of the drift velocity with increasing reduced electric fields. The existence of NDC for mixtures has been observed and understood previously [100–102], and arises for certain combinations of momentum and energy transfer rates. The addition of a small fraction of water to argon then begins to modify the energy transfer via the substantial rotational and vibrational processes present, and presents the necessary conditions for NDC to arise.

In this process, we can assess the self-consistency of the electron-water cross-section set proposed in [8]. We should emphasise that anisotropic scattering is considered in both the elastic and rotational cross-sections. Superelastic scattering processes in water are considered through thermally excited rotational state populations calculated according to Boltzmann statistics. The reader is referred to [8] for further details. For argon, we utilise the cross-section set proposed by Biagi

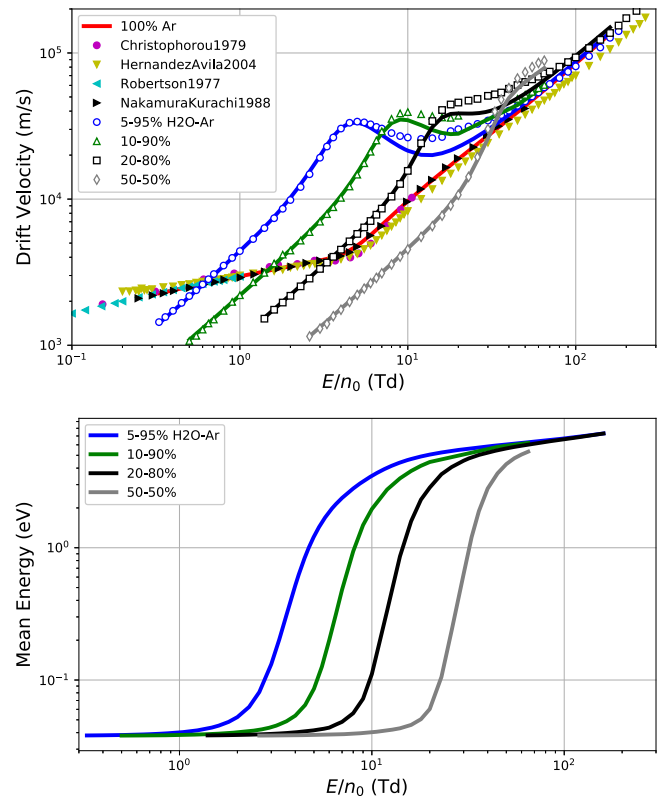


**Figure 3.** Variation of the drift velocities (top) and mean energy (bottom) of electrons with reduced electric field  $E/n_0$  for varying water–argon mixture ratios. The symbols represent the measured values using the current pulsed-Townsend technique while the solid lines represent the calculated values from a multi-term Boltzmann equation solution using the water vapour cross-section set proposed in [8]. See legend in figure for further details.

(MAGBOLTZ V8), for which self-consistency has been recently assessed [103].

We observe from figure 3 that the set of water vapour cross-sections proposed in [8] is consistent with the new water–argon mixture data in the low-energy and high-energy regimes. The set describes the NDC present in the 5% and 10% water cases, however it also predicts (albeit a weak one) NDC in the 20% case which is not observed experimentally. In the intermediate energy regimes, the calculated NDC predicted is more pronounced than observed experimentally. The largest discrepancies between the calculated and measured data appear in the intermediate energy regimes where the mean swarm energies are in the range of 2–5 eV as shown in figure 3. This indicates that further assessment/refinement is required in developing a self-consistent cross-section set. We also highlight there is other physics which should possibly be investigated.

In figure 3, we observe the presence of a ‘quasi-runaway’ regions for the various mixtures. This is highlighted by the regions of rapid increase in the mean energy of the electron swarm with increasing reduced electric field, and is indicative of cross-sections which are falling off sufficiently rapidly with energy. From a numerical calculation of transport coefficients viewpoint, this manifests itself as poor convergence rates, or

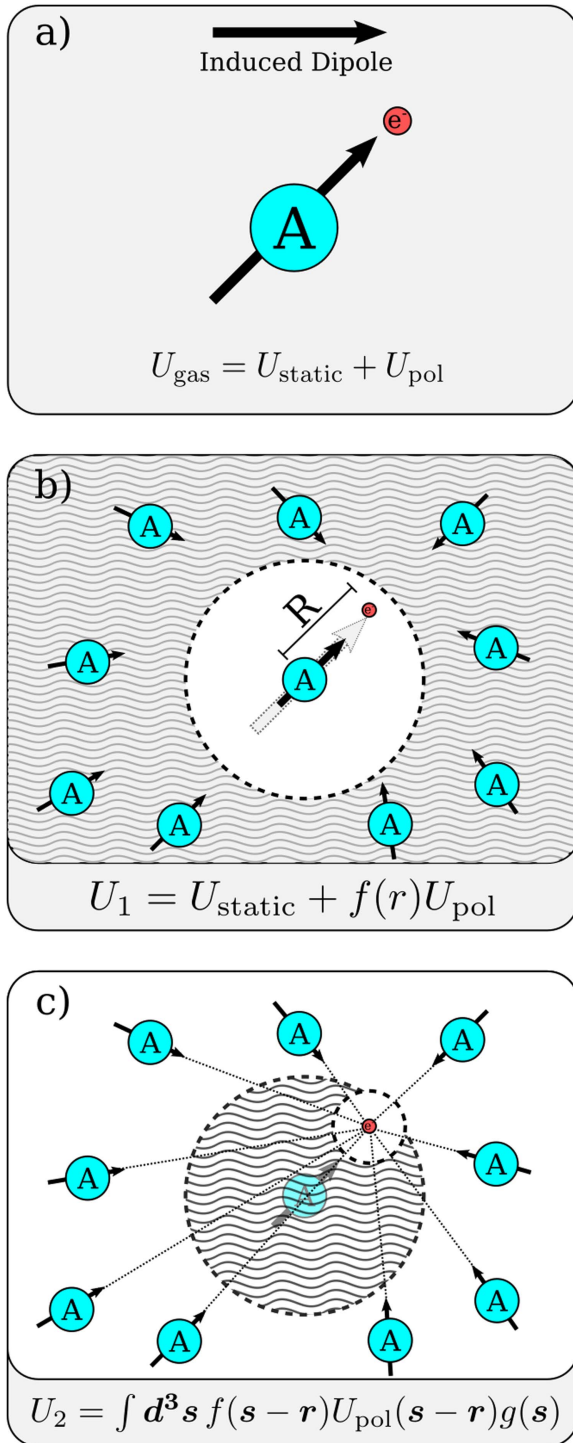


**Figure 4.** Schematic representation of the various components of the screening of the electron–atom potential in a liquid environment. (a) Gas phase potential is a combination of the static interaction potential  $U_{\text{static}}$  and the polarisation component  $U_{\text{pol}}$ . (b) Interaction potential  $U_1$  associated with the ‘focus atom’ is a combination of  $U_{\text{static}}$  and the polarisation potential screened by the surrounding atoms. (c) Interaction potential  $U_2$  associated with the surrounding atoms. Here  $\mathbf{r}$  denotes the position of the electron and  $\mathbf{s}$  the position of surrounding atoms.

convergence that is very sensitive to the numerical technique parameters. This was recently discussed in [104, 105]. Furthermore, it could be that in this small region of  $E/n_0$  the hydrodynamic approximation breaks down, and drift and

diffusion coefficients alone may not be sufficient to describe the current trace. These regions of  $E/n_0$  warrant further investigation, and resolution may be achieved in this region using a Monte Carlo technique [106] or space-time non-hydrodynamic Boltzmann equation solution [107] to simulate directly the form of the displacement current in the external circuit and compare with the measured current trace.

#### 4. Electron swarms in atomic liquids

As we strive towards a treatment of non-equilibrium electron transport in soft-condensed biological matter, we need to be able to translate and adapt the information gained from the electron-molecule interactions in the gas phase to the soft-condensed phase. As detailed above, the treatment of electron transport in liquids involves distinctly more complicated physical processes than in the gaseous and crystalline phases. The randomness assumption inbuilt in the theoretical treatment of gases is no longer present, and neither is the long-range order generally present in crystalline materials. Rather in liquids there exists some short range order, where the scattering centres are spatially and temporally correlated. For electrons in liquids and dense gases, we often have the situation where the de Broglie wavelength of the electron is of the order of the average inter-particle spacing  $\sim n_0^{-1/3}$ . In this regime, the electron can no longer be considered as a point particle, and must be treated as a wave, coherently scattering from scattering centres which are temporally and spatially correlated. Furthermore, in these phases the electron–atom interaction potential is modified from that in the dilute gas phase through screening effects. In what follows, we detail an *ab initio* formulation that adapts the gas phase treatment and addresses the additional complexity associated with treating electrons in liquid environments [81, 82].

##### 4.1. Coherent scattering effects

In previous studies the development of a collision operator in the multi-term formalism was presented that accurately treats the effects of coherent elastic scattering present in liquids and dense matter [108, 109]. An expression for the adjoint collision operator was developed from the definition of the double differential cross-section where it was represented in terms of the product of the single particle (screened) differential cross-sections and the dynamic structure factor [110]. In summary, the spherical harmonic projections of the elastic collision operator, in the small mass ratio limit, accounting for coherent scattering, are given by:

$$J^0(f_0^{(0)}) = \frac{m}{m_0 v^2} \frac{d}{dv} \left\{ v \nu_1(v) \left[ v f_0^{(0)} + \frac{kT}{m} \frac{d}{dv} f_0^{(0)} \right] \right\}, \quad (10)$$

$$J^l f_m^{(l)} = \tilde{\nu}_l(v) f_m^{(l)} \quad \text{for } l \geq 1, \quad (11)$$

where  $m_0$  is the mass of the atom, and

$$\nu_l(v) = n_0 v 2\pi \int_0^\pi \sigma(v, \chi) [1 - P_l(\cos \chi)] \sin \chi d\chi, \quad (12)$$



is the binary  $l$ th order transfer collision frequency in the absence of coherent scattering effects with  $\sigma(v, \chi)$  representing the (screened) differential scattering cross-section. In addition,

$$\tilde{\nu}_l(v) = n_0 v \left( 2\pi \int_0^\pi \Sigma(v, \chi) [1 - P_l(\cos \chi)] \sin \chi d\chi \right) \quad (13)$$

are the structure-modified higher-order collision frequencies that account for coherent scattering [109], while

$$\Sigma(v, \chi) = \sigma(v, \chi) S \left( \frac{2mv}{\hbar} \sin \frac{\chi}{2} \right), \quad (14)$$

represents an effective differential cross-section and  $S$  is the static structure factor. The static structure factor is a measurable quantity and can also be determined from the pair-correlator. In what follows we also define the momentum transfer collision frequencies without and with coherent scattering via  $\nu_1(v) = n_0 v \sigma_m(v)$  and  $\tilde{\nu}_1(v) = n_0 v \Sigma_m(v)$ , respectively. In a two-term framework only these can be sampled. The multi-term solution procedure enables higher-order components of the differential cross-sections to be sampled. The reader is referred to [81, 109] for further details.

#### 4.2. Screening of the scattering potential and ab initio calculation of liquid-phase scattering cross-sections

While the coherent scattering of an electron takes into account that the electron wavepacket extends over many atoms, exhibiting interference in elastic scattering processes, this only addresses part of the multiple scattering features that take place in dense media. We must also account for the scattering environment of each individual atom, which is modified by the presence of the surrounding atoms. In particular we would like to include effects of polarisation screening and the overlap of the surrounding atom potentials.

Figure 4 depicts these contributions. An isolated atom (see figure 4(a)) feels a potential due to a test charge placed nearby. This potential can be broken into a static part from the ground state of the atom and a polarisation contribution which results from the test charge inducing a multipole structure in the atom. In the liquid this atom, denoted as the ‘focus atom’ to distinguish it from its surrounds, also senses the multipoles that are induced in the surrounding atoms. The major contribution comes from the induced dipole of the atom. As the majority of these dipoles in the surrounds are oriented against the focus atom’s dipole, the overall effect is to screen the focus atom’s dipole, making the polarisation contribution weaker. We obtain this screening function  $f(r)$ , where  $r$  is the distance of the electron from the focus atom, by averaging over the surrounding atomic positions and solving the self-consistent equation:

$$f(r) = 1 - \pi N \int_0^\infty ds \frac{g(s)}{s^2} \int_{|r-s|}^{r+s} dt \Theta(r, s, t) \frac{\alpha_d(t) f(t)}{t^2}. \quad (15)$$

Here  $g(s)$  is the pair-correlator,  $\alpha_d(t)$  is the dipole polarisability for an electron at a distance  $t$  from an isolated atom

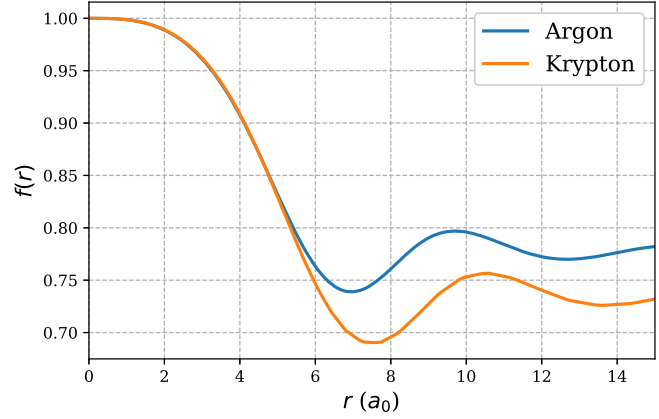


**Figure 5.** The screening function  $f(r)$  of the polarization interaction potential for scattering of an electron from a single atom: of argon ( $n_0 = 0.0213 \text{ \AA}^{-3}$ ) and krypton ( $n_0 = 0.0172 \text{ \AA}^{-3}$ ).

and

$$\Theta(r, s, t) = \frac{3(s^2 + t^2 - r^2)(s^2 + r^2 - t^2)}{2s^2 + (r^2 + t^2 - s^2)}. \quad (16)$$

The screening function is shown in figure 5 for various atomic liquids. In the limit of  $r \rightarrow 0$  the spherical symmetry of the surrounding atoms causes no screening to occur. In the limit of  $r \rightarrow \infty$ , the screening is related to the dielectric constant of the liquid and is given by the Lorentz factor,  $f_L = \left[ 1 + \frac{8}{3} \pi N \alpha_d(r \rightarrow \infty) \right]^{-1}$ .

The screening affects the polarisation potential of the focus atom. The other major contribution from the surrounding atoms is to modify the total scattering potential (see figure 4). This is because the atoms are close enough together that the electron always feels a varying potential from more than one atom. The total potential ( $U_{\text{eff}} = U_1 + U_2$ ) is made up of the combined focus ( $U_1$ ) and surrounding ( $U_2$ ) potentials. After averaging over the surrounding atomic distribution, we find:

$$U_2(r) = \frac{2\pi N}{r} \int_0^\infty dt t U_1(t) \int_{|r-t|}^{r+t} ds s g(s). \quad (17)$$

An example of  $U_1$ ,  $U_2$  and their combination is shown in figure 6 for scattering from atoms in liquid krypton. The strong static attraction dominates for short distances, where the contribution of the surrounding atoms is relatively constant. At around half of the average separation between the atoms, the contributions from the focus and surrounding atoms become roughly equal.

The presence of the surrounding atoms also mean that the scattering problem cannot be solved with asymptotic plane waves as the boundary conditions. Instead we consider that each atom has a spherical scattering cell, of size  $r_m$ . We choose  $r_m$  to be the first turning point of the combined potential (see figure 6) with the goal of finding a good representation of the free volume in which the electron can move.

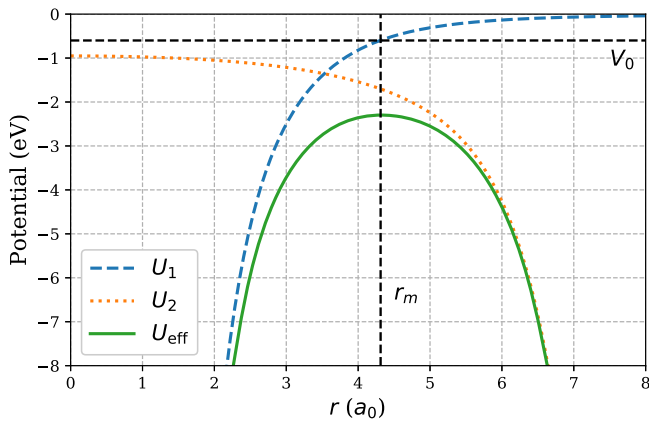


**Figure 6.** The total effective potential  $U_{\text{eff}}$  felt by an electron when colliding with one krypton atom. Also shown are the components,  $U_1$  and  $U_2$ , which represent the direct potential of the atom and the contribution of the remaining atoms in the bulk respectively. The dashed vertical line indicates the (Lekner) proposed collisional sphere radius,  $r_m$ . The effects of exchange are not represented in this figure. We find that a shift  $V_0$  is required, which is indicated by a dashed horizontal line (see text).

The liquid-phase cross-sections are calculated using the Dirac scattering equations including both static and dynamic polarization potentials as determined by the polarized-orbital method [111–113]. We consider the full multipole polarization potential and a true non-local treatment of exchange. The accuracy of the interaction potential is assessed through comparison with the measured (benchmarked) gas phase cross-sections. In contrast to previous investigations, our process involves a complete treatment of the static and polarisation parts of the potential including the screening component and a non-local treatment of exchange, for both the focus and surrounding atoms. For further details the reader is referred to [81, 82].

#### 4.3. Electron cross-sections and transport in liquid Ar

As a demonstration of the implementation of the above *ab initio* framework we consider electrons in liquid argon. In figure 7, we present the electron–argon scattering cross-sections in the gas and liquid phases using the formalism detailed above. We compare the dilute gas phase cross-section with the benchmark cross-sections of Buckman *et al* [114], and the agreement confirms the validity of the electron–argon scattering potential and solution technique. We observe that the effect of the screening is to remove the presence of the Ramsauer minimum in the cross-section, making the cross-section essentially independent of energy at low incident electron energies. The inclusion of coherent scattering is seen to reduce the momentum transfer cross-section at low-energies. At higher energies, where the de Broglie wavelength is reduced below the inter-pa10.1088 separation, the liquid-phase cross-section approaches the dilute gas phase cross-section.

In figure 8, we present the calculated drift velocity and characteristic energy of electrons in liquid argon using cross-sections developed using the formalism detailed above

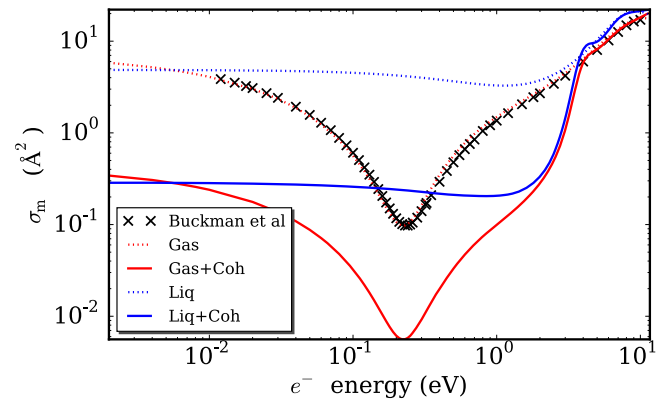


**Figure 7.** The momentum transfer cross-sections in the gas phase (Gas), liquid-phase (Liq) and their modifications when coherent scattering effects are included (+Coh). The recommended momentum transfer cross-section of reference [114] for a dilute gas is a combination of experimental measurements and theoretical calculations. (Source: Reproduced from [81], with the permission of AIP Publishing.)

[81, 82] and the multi-term Boltzmann equation solution framework. The results are compared with the available experimental data. Transport properties are presented as a function of the reduced electric field, and thus extract out the explicit density dependence. The results demonstrate the inadequacy of treating transport in liquids through the dilute gas cross-sections and transport theory scaled by the liquid density. The accuracy of the gas phase cross-section (and hence electron–argon interaction potential) is once again confirmed for transport in the dilute gas phase. The results highlight the ability of our *ab initio* technique to calculate liquid-phase cross-sections and associated transport properties. In figure 8, we also highlight the explicit impact of coherent scattering and screening separately, and demonstrate that both effects are required to accurately represent the transport [81].

In a recent study [82], the same *ab initio* procedure was applied to electrons in liquid xenon and was demonstrated to have similar levels of agreement. In the following section, we apply the procedure to liquid krypton for the first time.

#### 4.4. Electrons in liquid Kr

In figure 9, we present the electron impact cross-sections for liquid krypton using the *ab initio* procedure detailed in section 4.1. A comparison of the calculated gas phase cross-section with the benchmark cross-section of Biagi [123], gives a representative indication of the accuracy of the electron–krypton interaction potential and associated cross-section, and this is supported in the comparison of the calculated drift velocities with the experimental values available in the literature (see [123, 124] and references therein). Application of the *ab initio* screening procedure again results in suppression of the Ramsauer minimum in the momentum transfer cross-section. This is consistent with the procedure implemented by Atrazhev and co-workers [48], however the value of the low-energy cross-section deviates substantially from their value. In figure 10, we compare the drift velocities

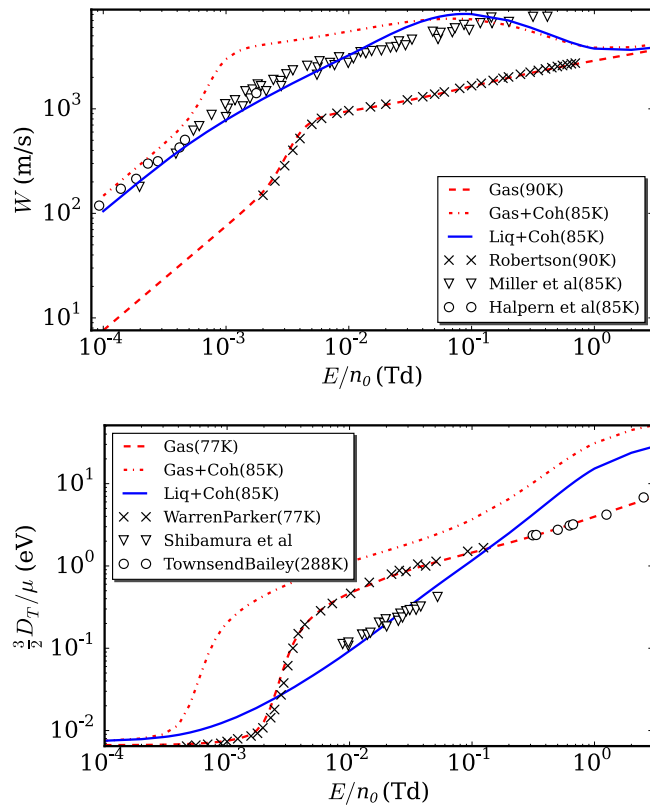


**Figure 8.** Comparison of the measured drift velocities  $W$  (top) and characteristic energies  $D_T/\mu$  (bottom) in gaseous and liquid argon, with those calculated from the various approximations to the cross-sections. Experimental data—Ar: Robertson [115, 116] at 90 K; Miller *et al* [117] at 85 K; Halpern *et al* [118] at 85 K; Warren and Parker [119, 120] at 77 K; Townsend and Bailey [119, 121] at 288 K; Shibamura *et al* [122] at an unmeasured liquid temperature. The various approximations used are: gas phase only cross-sections (Gas), gas phase cross-sections with coherent scattering (Gas+Coh), and liquid-phase cross-sections with coherent scattering effects (Liq+Coh). The results have been calculated using the full differential cross-section and results are converged multi-term values. (Source: Reproduced from [81], with the permission of AIP Publishing.)

calculated using the *ab initio* cross-sections with the available experimental data [117, 125]. We can see immediately that our results are inconsistent with experiment, particularly at low reduced fields. Although the gas phase results indicate that there are some small issues with the electron–krypton interaction potential and associated cross-sections, it is clear that the *ab initio* framework presented above fails to capture some essential physics in the particular case of liquid krypton.

We subsequently began to investigate some of the parameters that are specified in the calculation of the liquid-phase scattering cross-sections.

One parameter that has attracted much investigation in the literature is  $V_0$ , generally referred to as the background energy of the electron in the liquid [61, 65, 128, 129]. This is likened to the bottom of the conduction band for electrons in a liquid, in analogy with solid state band-structure. For the purposes of our scattering calculation, this modifies the asymptotic energy of the electron. Instead of asymptoting to  $\epsilon = \hbar^2 k^2 / 2m$  as  $r \rightarrow \infty$  for a single atom scattering

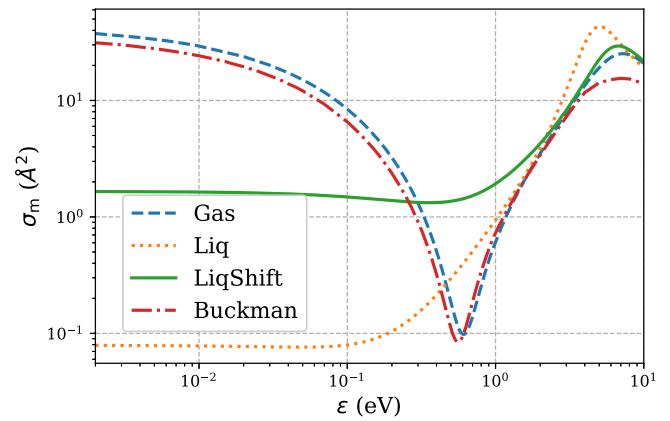


**Figure 9.** The electron–krypton momentum transfer cross-sections in the gas phase (Gas) and liquid-phase (Liq and LiqShift) without coherent effects. The standard procedure (Liq) appears to produce cross-sections that are much too small. To address this, we apply a shift (LiqShift, see text) which better matches experimental results. The modifications due to coherent effects (not shown) are the same for both liquid cross-sections. The recommended gas phase momentum transfer cross-section (Buckman) is from reference [114].

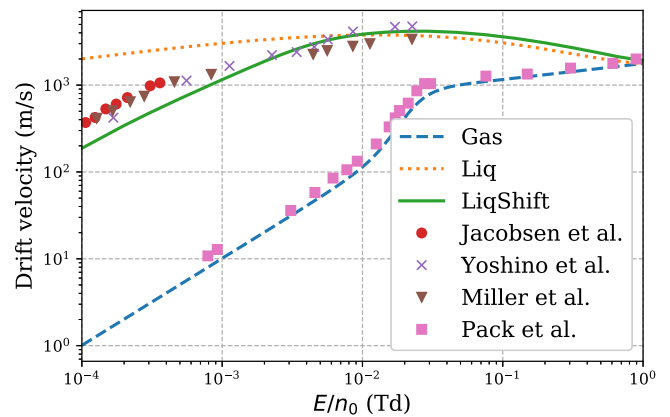


**Figure 10.** Comparison of the calculated drift velocities  $W$  of electrons in gaseous and liquid krypton with the available experimental data (Gas: Pack *et al* [123, 124] and references therein; Liquid: Miller *et al* [117], Schnyders *et al* [125], Jacobsen *et al* [126], Yoshino *et al* [127]). The standard procedure (Liq) results in drifts that are too large compared with experiment. By applying an energy shift (LiqShift, see text) we can obtain reasonable agreement with experiment. The transport coefficients are converged multi-term values.

calculation, we now have the electron asymptoting to  $\epsilon = V_0 + \hbar^2 k^2 / 2m$  as  $r \rightarrow r_m$ .

There have been field-ionisation experiments which have extracted the value of  $V_0$  for krypton over a range of densities [65], and consequently we use the approximate value of  $V_0 = -0.6$  eV in this study. We then shift our scattering potential by this amount to account for the changed asymptote. We see in figure 9 that this predominantly raises the low-energy part of the liquid-phase cross-section. Consequently, we find in figure 10 that calculated drift velocity in the low-field regime then decreases in line with experimental data. The calculated drift velocity still slightly underestimates the

experimental data, however this is consistent with the gas phase results used to assess the interaction potential.

There is an obvious discrepancy between the approach required here for krypton and our previous investigations of liquid argon and liquid xenon [81, 82]. In the language of this study, our previous investigations applied a ‘zero shift’ of  $V_0 = 0$ . As there are also field-ionisation measurements for argon [65], we have repeated those calculations for argon using the experimental value of  $V_0$  but found that the transport quantities were pushed in the wrong direction producing disagreement between the calculations and measurements. However, we also find that we can choose a non-zero value of  $V_0$  shift empirically that matches well with the transport measurements. That is, there exist two possible shifts (one of which is approximately zero for argon) which produce transport quantities that differ slightly but are in close agreement with each other and the experimental transport measurements. This will be the focus of future work where we directly probe  $V_0$  in our formalism, which may expose subtle differences to the experimentally measured values of  $V_0$ .

## 5. Other physical processes in liquids

Experimental evidence of electron transport in soft-condensed matter indicates that more complex physics is required to be included in addition to the above traditional scattering processes [61, 72–79]. More specifically, electrons can be solvated within the liquid/soft-condensed matter through a variety of mechanisms, including self-trapping into localised bubble or solvated states (even for non-polar liquids) [61, 72–79].

For atomic liquids, experimental and theoretical evidence further suggests that these states can be weakly bound [41, 61, 72, 73]. The study of Sakai *et al* [41] is particularly noteworthy here. Considering electrons in liquid neon, their experimental results exhibit what is known as dispersive, anomalous or fractional transport [130, 131], where the current trace for a certain range of fields exhibits two distinct power-law components at short and long times (see figure 14 of [41]). Such current transients are ubiquitous in charge transport in amorphous and organic materials (so called Scher–Montroll behaviour [132]), and reflect a process of trapping and detrapping of charged pa10.1088s. Consequently, in addition to the capture events of the electrons into localised states within the liquid, they can be followed by subsequent detrapping back into delocalised transport states at a later time. A phase-space depiction of this is schematically represented in figure 11. We have recently developed a generalised Boltzmann equation that is capable of capturing these trapping and detrapping processes, accounting for the combined localised–delocalised nature of electron transport exhibited in these materials. The generalised Boltzmann equation for the free pa10.1088 phase-space distribution

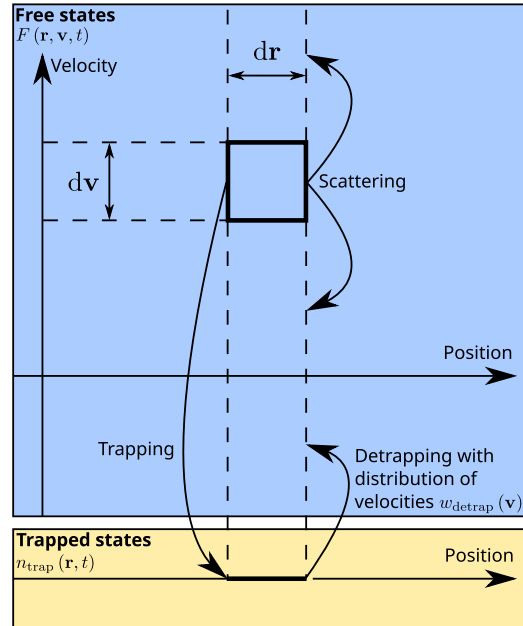


**Figure 11.** Phase-space diagram illustrating the combined localised–delocalised nature of transport in liquids and soft-matter, with scattering events combined with scattering into localised trap states, and subsequent detrapping processes with a specified velocity distribution.

function  $f(\mathbf{r}, \mathbf{v}, t)$  is given by [83]

$$\left( \frac{\partial}{\partial t} + \mathbf{v} \cdot \frac{\partial}{\partial \mathbf{r}} + \frac{e\mathbf{E}}{m} \cdot \frac{\partial}{\partial \mathbf{v}} \right) F(\mathbf{r}, \mathbf{v}, t) = -J(F) - \nu_{\text{trap}}(\mathbf{v})F(\mathbf{r}, \mathbf{v}, t) + \Phi(t)^*[n(\mathbf{r}, t)\langle \nu_{\text{trap}}(\mathbf{v}) \rangle] \tilde{w}_{\text{detrap}}(\mathbf{v}). \quad (18)$$

The second term on the right hand side represents the loss of free pa10.1088s to trapped states, while the third term represents the return of these electrons back to the delocalised states at a later time with a specific velocity distribution function  $\tilde{w}_{\text{detrap}}(\mathbf{v})$ . Here, trapping losses are characterised by the trapping frequency  $\nu_{\text{trap}}(\mathbf{v})$  (determined by the trapping cross-sections),  $*$  denotes a convolution in time,  $\langle \cdot \rangle$  denotes an average over velocity space and  $n(\mathbf{r}, t)$  represents the free pa10.1088 number density which is defined through  $n(\mathbf{r}, t) \equiv \int F(\mathbf{r}, \mathbf{v}, t) d\mathbf{v}$ . The residence time in the trapped or localised state is sampled from the effective waiting time distribution [83]:

$$\Phi(t) \equiv e^{-\nu_{\text{loss}}^{(\text{trap})} t} \phi(t), \quad (19)$$

defined in terms of a trapping time distribution  $\phi(t)$  and weighted by an exponential decay term that describes the possibility of recombination of trapped pa10.1088s at the rate  $\nu_{\text{loss}}^{(\text{trap})}$  [83]. The trapping time distribution is calculable from the density of trapped states in the liquid. For simplicity, the processes of detrapping are taken to be isotropic and to take the form of Maxwellian-type velocity distributions. Specifically, we introduce:

$$\tilde{w}_{\text{detrap}}(\mathbf{v}) \equiv \frac{\nu_{\text{trap}}(\epsilon) w(\alpha_{\text{detrap}}, \mathbf{v})}{\int d\mathbf{v} \nu_{\text{trap}}(\epsilon) w(\alpha_{\text{detrap}}, \mathbf{v})}, \quad (20)$$



where the Maxwellian velocity distribution of temperature  $T$  is defined as:

$$w(\alpha, v) \equiv \left(\frac{\alpha^2}{2\pi}\right)^{\frac{3}{2}} \exp\left(-\frac{\alpha^2 v^2}{2}\right), \quad (21)$$

$$\alpha^2 \equiv \frac{m}{kT}, \quad (22)$$

where  $k$  is the Boltzmann constant.

In [83, 133], we demonstrated that a steady-state solution of (18) for the velocity distribution for particular functional forms of the distribution of trapping times  $\phi(t)$  was able to reproduce the Scher–Montroll current traces and hence the dispersive nature of transport in these systems. An ability to extract  $\phi(t)$  enables an understanding of the density of trapped states in energy space. Whilst we could fit the current trace to these solutions and hence extract out the functional form of the trapping time distribution and the trapping rates  $\nu_{\text{trap}}$ , our goal is to develop an *ab initio* method for calculating these quantities. Recently, we have made progress towards this goal, postulating electron capture into local fluctuations in the liquids as the mechanism of self-trapping bubble/cluster formation. The probability of scattering into these fluctuations (which determines  $\nu_{\text{trap}}$ ) and the subsequent stability of these ‘bubbles/clusters’ (which determine  $\phi(t)$ ) are calculable in an *ab initio* manner. The reader is referred to [134] for details.

## 6. Conclusion

In this study we present progress towards a generalised framework for the modelling of non-equilibrium electron transport in liquids and soft-condensed matter. The framework is based on generalisation of Boltzmann’s equation to account for various processes present in such matter including coherent scattering processes, interaction potential modification and the combined localised–delocalised nature of the transport.

For plasma interactions with biological matter, the development of self-consistent cross-sections is imperative. In this study, we have presented self-consistency checks for electron-water and electron-THF cross-section sets in the pure gaseous forms, as well as in mixtures with atomic gases. The swarm studies of water vapour in mixtures with atomic (and/or molecular) gases represents an important check on the self-consistency of the electron-water vapour cross-section set. Importantly, it goes part way to removing the degeneracy in the cross-section sets i.e., various cross-section sets can

produce the same transport coefficients. The electron-water vapour cross-section presented in [8] identified some minor issues in the intermediate energy range (1–5 eV mean energies) present in the water–argon mixtures that were not observed in the water–helium mixtures. This warrants further investigation, including an assessment of the impact of ‘quasi-runaway’ at the fields where the discrepancies are largest. The next phase of this work is to consider water vapour in other mixtures (e.g. molecular nitrogen). Likewise, the degeneracy and self-consistency of the electron-THF cross-section set proposed in [19] needs an equivalent interrogation using atomic and molecular admixtures.

The extension to consider transport in liquids and soft-condensed matter represents a grand challenge within the field. Even for simple high-mobility atomic liquids, there is still much physics which is unknown and requires further attention. While our *ab initio* theory has been shown to work well for argon and xenon, in the current study we have shown that further physics is required for krypton. For low-mobility atomic liquids, we have presented a Boltzmann equation framework that accounts for the combined localised–delocalised nature of the transport experimentally demonstrated to exist in some liquids. Further work is required for the *ab initio* calculation of the trapping and detrapping rates for implementation. As we move to consider the long-range interactions present in dipolar liquids such as water etc, further physics will need to be included for any non-equilibrium transport modelling. The transition to solvation under non-equilibrium conditions remains a key question in this field [3, 75].

## Acknowledgments

The authors would like to thank the Australian Research Council through its Discovery (grant numbers DP160102787 and DP180101655) and Centres of Excellence programs for financial support and the Australian Academy of Science through its European Scientific Exchange Program. We also thank A Bustos, H Hinojosa and G Bustos for their technical assistance on the experimental component. The experimental part was supported by a grant from the Mexican government through Project Conacyt 240073 and PAPIIT IN 111014. SD and ZLjP would like to acknowledge MPNTR projects ON171037 and III41011 for support.



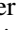
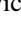
## Appendix



**Table A1.** Experimentally measured drift velocities for electrons in Ar–water mixtures using the pulsed-Townsend experiment.

95% Ar–5% Water			90% Ar–10% Water			80% Ar–20% Water			50% Ar–50% Water		
$E/n_0$ (Td)	$W$ (cm s <sup>-1</sup> )	Error (cm s <sup>-1</sup> )	$E/n_0$ (Td)	$W$ (cm s <sup>-1</sup> )	Error (cm s <sup>-1</sup> )	$E/n_0$ (Td)	$W$ (cm s <sup>-1</sup> )	Error (cm s <sup>-1</sup> )	$E/n_0$ (Td)	$W$ (cm s <sup>-1</sup> )	Error (cm s <sup>-1</sup> )
0.33	144000	2160	0.5	107000	1605	1.4	152000	2280	2.6	115000	2300
0.36	156000	2340	0.55	116000	1740	1.6	175000	2625	3	130000	2600
0.4	172000	2580	0.6	128000	1920	1.8	196000	2940	3.3	140000	2800
0.45	195000	2925	0.65	141000	2115	2	218000	3270	3.6	158000	3160
0.5	217000	3255	0.7	150000	2250	2.3	253000	3795	4	175000	3500
0.55	238000	3570	0.8	172000	2580	2.6	286000	4290	4.5	198000	3960
0.6	261000	3915	0.9	198000	2970	3	333000	4995	5	221000	4420
0.65	283000	4245	1	220000	3300	3.3	368000	5520	5.5	244000	4880
0.7	307000	4605	1.2	270000	4050	3.6	403000	6045	6	266000	5320
0.8	351000	5265	1.4	313000	4695	4	451000	6765	6.5	289000	5780
0.9	396000	5940	1.6	363000	5445	4.5	514000	7710	7	311000	6220
1	441000	6615	1.8	417000	6255	5	578000	8670	8	357000	7140
1.2	533000	7995	2	445000	6675	5.5	640000	9600	9	404000	8080
1.4	633000	9495	2.3	520000	7800	6	708000	10620	10	453000	9060
1.6	740000	11100	2.6	595000	8925	6.5	782000	11730	12	552000	11040
1.8	859000	12885	3	701000	10515	7	861000	12915	14	653000	13060
2	986000	14790	3.3	789000	11835	8	1040000	15600	16	770000	15400
2.3	1210000	18150	3.6	880000	13200	9	1270000	19050	18	903000	18060
2.6	1480000	22200	4	1020000	15300	10	1560000	23400	20	1070000	21400
3	1920000	28800	4.5	1220000	18300	12	2410000	36150	23	1420000	28400
3.3	2290000	34350	5	1470000	22050	14	3420000	51300	26	1940000	38800
3.6	2640000	39600	5.5	1760000	26400	16	4070000	61050	30	3020000	60400
4	3040000	45600	6	2110000	31650	18	4440000	66600	33	3970000	79400
4.5	3330000	49950	6.5	2520000	37800	20	4580000	68700	36	4800000	96000
5	3390000	50850	7	2910000	43650	23	4720000	70800	40	5750000	115000
5.5	3350000	50250	8	3540000	53100	26	4850000	72750	45	6690000	133800
6	3250000	48750	9	3860000	57900	30	5090000	76350	50	7380000	147600
6.5	3120000	46800	10	3940000	59100	33	5210000	78150	55	8000000	160000
7	3040000	45600	12	3810000	57150	36	5360000	80400	60	8550000	171000
8	2830000	42450	14	3700000	55500	40	5690000	85350	65	8860000	177200
9	2700000	40500	16	3620000	54300	45	6030000	90450			
10	2640000	39600	18	3600000	54000	50	6330000	94950			
12	2580000	38700	20	3720000	55800	55	6600000	99000			
14	2610000	39150	45	4850000	72750	60	6880000	103200			
16	2660000	39900	50	5170000	77550	65	7240000	108600			
18	2920000	46050	55	5420000	81300	70	7450000	111750			
20	3010000	45150	60	5740000	86100	80	8050000	120750			
23	3140000	47100	65	6040000	90600	90	8660000	129900			
26	3270000	49050				100	9330000	139950			
30	3450000	51750				120	10800000	162000			
33	3610000	54150				140	12300000	184500			
36	3760000	56400				160	13700000	205500			
40	4030000	60450				180	15400000	231000			
45	4350000	65250				200	17300000	259500			
50	4670000	70050				230	19400000	291000			
55	5040000	75600				260	21800000	327000			
60	5370000	80550									
65	5810000	87150									
70	6140000	92100									
80	6740000	101100									
90	7430000	111450									
100	8100000	121500									
120	9510000	142650									
140	10900000	163500									
160	12700000	190500									
180	14100000	211500									

## ORCID iDs

R D White  <https://orcid.org/0000-0001-5353-7440>  
 D Cocks  <https://orcid.org/0000-0002-9943-7100>  
 N Garland  <https://orcid.org/0000-0003-0343-0199>  
 M J Brunger  <https://orcid.org/0000-0002-7743-2990>  
 Z Lj Petrovic  <https://orcid.org/0000-0001-6569-9447>

## References

- [1] Samukawa S *et al* 2012 *J. Phys. D: Appl. Phys.* **45** 253001
- [2] Bruggeman P J *et al* 2016 *Plasma Sources Sci. Technol.* **25** 053002
- [3] Adamovich I *et al* 2017 *J. Phys. D: Appl. Phys.* **50** 323001
- [4] Alizadeh E, Orlando T M and Sanche L 2015 *Annu. Rev. Phys. Chem.* **66** 379
- [5] Aouchiche H, Champion C and Oubaziz D 2008 *Radiat. Phys. Chem.* **77** 107
- [6] Blanco F, Muñoz A, Almeida D, Silva F F D, Limão-Vieira P and García G 2014 *Int. J. Mass Spectrom.* **365–366** 287
- [7] Date H, Sutherland K L, Hasegawa H and Shimozuma M 2007 *Nucl. Instrum. Methods Phys. Res. B* **265** 515
- [8] de Urquijo J, Basurto E, Juárez A M, Ness K F, Robson R E, Brunger M J and White R D 2014 *J. Chem. Phys.* **141** 014308
- [9] Hasegawa H, Date H and Shimozuma M 2007 *J. Phys. D: Appl. Phys.* **40** 2495
- [10] Itikawa Y and Mason N 2005 *J. Phys. Chem. Ref. Data* **34** 1
- [11] Khakoo M, Winstead C and McKoy V 2009 *Phys. Rev. A* **79** 052711
- [12] Ness K F, Robson R E, Brunger M J and White R D 2012 *J. Chem. Phys.* **136** 024318
- [13] Robson R E, White R D and Ness K F 2011 *J. Chem. Phys.* **134** 064319
- [14] Thorn P, Campbell L and Brunger M 2009 *PMC Phys. B* **2** 1
- [15] Yousofi M and Benabdessadok M D 1996 *J. Appl. Phys.* **80** 6619
- [16] Zhang R, Faure A and Tennyson J 2009 *Phys. Scr.* **80** 015301
- [17] Garland N A, Brunger M J, Garcia G, de Urquijo J and White R D 2013 *Phys. Rev. A* **88** 062712
- [18] White R D, Brunger M J, Garland N A, Robson R E, Ness K F, García G, de Urquijo J, Dujko S and Petrović Z L 2014 *Eur. Phys. J. D* **68** 125
- [19] Casey M J E, de Urquijo J, Loli L N S, Cocks D G, Boyle G J, Jones D B, Brunger M J and White R D 2017 *J. Chem. Phys.* **147** 195103
- [20] Chiari L *et al* 2013 *J. Chem. Phys.* **138** 074301
- [21] Fuss M C, Sanz A G, Blanco F, Limão-Vieira P, Brunger M J and García G 2014 *Eur. Phys. J. D* **68** 161
- [22] Trevisan C S, Orel A E and Rescigno T N 2006 *J. Phys. B: At. Mol. Opt. Phys.* **39** L255
- [23] Jones D, Builth-Williams J, Bellm S, Chiari L, Chaluvadi H, Madison D, Ning C, Lohmann B, Ingólfsson O and Brunger M 2013 *Chem. Phys. Lett.* **572** 32
- [24] Duque H V, Do T P T, Lopes M C A, Kononov D A, White R D, Brunger M J and Jones D B 2015 *J. Chem. Phys.* **142** 124307
- [25] Limão-Vieira P, Duffot D, Hubin-Franskin M J, Delwiche J, Hoffmann S V, Chiari L, Jones D B, Brunger M J and Lopes M C 2014 *J. Phys. Chem. A* **118** 6425
- [26] Milosavljević A R, Kocisek J, Papp P, Kubala D, Marinković B P, Mach P, Urban J and Matejčík S 2010 *J. Chem. Phys.* **132** 104308
- [27] Zecca A, Chiari L, García G, Blanco F, Trainotti E and Brunger M J 2011 *New J. Phys.* **13** 063019
- [28] Duque H V *et al* 2014 *J. Chem. Phys.* **140** 214306
- [29] Jones D B, Ellis-Gibblings L, García G, Nixon K L, Lopes M C A and Brunger M J 2015 *J. Chem. Phys.* **143** 094304
- [30] Do T P, Duque H V, Lopes M C, Kononov D A, White R D, Brunger M J and Jones D B 2015 *J. Chem. Phys.* **142** 124306
- [31] Chiari L *et al* 2014 *J. Chem. Phys.* **141** 024301
- [32] Brunger M J 2017 *Int. Rev. Phys. Chem.* **36** 333
- [33] Huxley L G H and Crompton R W 1974 *The Diffusion and Drift of Electrons in Gases* (New York: Wiley)
- [34] Crompton R 1994 *Adv. At. Mol. Opt. Phys.* **33** 97
- [35] Petrović Z L, Dujko S, Marić D, Malović G, Nikitović Ž, Šašić O, Jovanović J, Stojanović V and Radmilović-Radenović M 2009 *J. Phys. D: Appl. Phys.* **42** 194002
- [36] Petrović Z L, Šuvakov M, Nikitović Ž, Dujko S, Šašić O, Jovanović J, Malović G and Stojanović V 2007 *Plasma Sources Sci. Technol.* **16** S1
- [37] Ness K F and Robson R E 1988 *Phys. Rev. A* **38** 1446
- [38] Kawaguchi S, Takahashi K, Satoh K and Itoh H 2016 *Japan. J. Appl. Phys.* **55** 07LD03
- [39] Schmidt W 1984 *IEEE Trans. Electr. Insul.* **EI-19** 389
- [40] Lekner J 1967 *Phys. Rev.* **158** 103
- [41] Sakai Y and Schmidt W F 1992 *Chem. Phys.* **164** 139
- [42] Sakai Y, Nakamura S and Tagashira H 1985 *IEEE Trans. Electr. Insul.* **EI-20** 133
- [43] Sakai Y 2007 *J. Phys. D: Appl. Phys.* **40** R441
- [44] Borghesani A and Santini M 1990 *Meas. Sci. Technol.* **1** 939
- [45] Borghesani A F and O'Malley T F 2003 *J. Chem. Phys.* **118** 2760
- [46] Borghesani A F 2006 *IEEE Trans. Dielectr. Electr. Insul.* **13** 492
- [47] Borghesani A F and Lamp P 2011 *Plasma Sources Sci. Technol.* **20** 034001
- [48] Atrazhev V M and Iakubov I T 1981 *J. Phys. C: Solid State Phys.* **14** 5139
- [49] Atrazhev V and Timoshkin I 1996 *Phys. Rev. B* **54** 11252
- [50] Atrazhev V M and Timoshkin I V 1998 *IEEE Trans. Dielectr. Electr. Insul.* **5** 450
- [51] Cohen M and Lekner J 1967 *Phys. Rev.* **158** 305
- [52] Garland N A, Cocks D G, Boyle G J, Dujko S and White R D 2017 *Plasma Sources Sci. Technol.* **26** 075003
- [53] Garland N A, Boyle G J, Cocks D G and White R D 2018 *Plasma Sources Sci. Technol.* **27** 024002
- [54] Atrazhev V M, Iakubov I T and Roldughin V I 1976 *J. Phys. D: Appl. Phys.* **9** 1735
- [55] Atrazhev V M and Iakubov I T 1977 *J. Phys. D: Appl. Phys.* **10** 2155
- [56] Atrazhev V, Iakubov I and Pogosov V 1995 *Phys. Lett. A* **204** 393
- [57] Springett B E, Cohen M H and Jortner J 1967 *Phys. Rev.* **159** 183
- [58] Hernandez J P 1991 *Rev. Mod. Phys.* **63** 675
- [59] Nazin S and Shikin V 2005 *J. Exp. Theor. Phys. Lett.* **82** 236
- [60] Iakubov I T and Khrapak A G 1982 *Rep. Prog. Phys.* **45** 697
- [61] Nieminen R M, Välimaa I, Manninen M and Hautojärvi P 1980 *Phys. Rev. A* **21** 1677
- [62] Coker D F, Berne B J and Thirumalai D 1987 *J. Chem. Phys.* **86** 5689
- [63] Chen X and Kuang L-M 1994 *J. Phys. A: Math. Gen.* **27** L685
- [64] Evans C M, Krynski K, Streeter Z and Findley G L 2015 *J. Chem. Phys.* **143** 224303
- [65] Evans C M and Findley G L 2010 *Phys. Res. Int.* **1**
- [66] Braglia G and Dallacasa V 1982 *Phys. Rev. A* **26** 902
- [67] Polischuk A Y 1985 *J. Phys. B: At. Mol. Phys.* **18** 829

- [68] Polischuk A Y 1999 *J. Phys. B: At. Mol. Opt. Phys.* **16** 3853
- [69] Giraud V and Krebs P 1982 *Chem. Phys. Lett.* **86** 85
- [70] Krebs P and Vautrin S 1991 *J. Phys.* **C5** 115
- [71] Krebs P and Lang U 1996 *J. Phys. Chem.* **100** 10482
- [72] Maris H J 2003 *J. Low Temp. Phys.* **132** 77
- [73] Shkrob I A and Sauer M C 2005 *J. Chem. Phys.* **122**
- [74] Hung S S S and Freeman R 1978 *Can. J. Chem.* **56** 2388
- [75] Rumbach P, Bartels D M, Sankaran R M and Go D B 2015 *Nat. Commun.* **6** 7248
- [76] Abel B 2013 *Annu. Rev. Phys. Chem.* **64** 533
- [77] Gopalakrishnan R, Kawamura E, Lichtenberg A J, Lieberman M A and Graves D B 2016 *J. Phys. D: Appl. Phys.* **49** 295205
- [78] Siefertmann K R, Liu Y, Lugovoy E, Link O, Faubel M, Buck U, Winter B and Abel B 2010 *Nat. Chem.* **2** 274
- [79] Skorobogatiy M, Park I J and Joannopoulos J D 2005 *Comput. Mater. Sci.* **32** 96
- [80] Gallicchio E and Berne B J 1996 *J. Chem. Phys.* **105** 7064
- [81] Boyle G J, McEachran R P, Cocks D G and White R D 2015 *J. Chem. Phys.* **142** 154507
- [82] Boyle G J, McEachran R P, Cocks D G, Buckman S J, Dujko S and White R D 2016 *J. Phys. D: Appl. Phys.* **49** 355201
- [83] Stokes P W, Philippa B, Cocks D and White R D 2016 *Phys. Rev. E* **93** 1
- [84] Wang-Chang C S, Uhlenbeck G E and De Boer J 1964 *Studies in Statistical Mechanics* vol 2 (New York: Wiley) p 241
- [85] Ness K F and Robson R E 1986 *Phys. Rev. A* **34** 2185
- [86] Robson R E 1991 *Aust. J. Phys.* **44** 685
- [87] White R D, Robson R E, Dujko S, Nicoletopoulos P and Li B 2009 *J. Phys. D: Appl. Phys.* **42** 194001
- [88] White R D, Dujko S, Robson R E, Petrović Z L and McEachran R P 2010 *Plasma Sources Sci. Technol.* **19** 034001
- [89] Boyle G J, Tattersall W J, Cocks D G, Dujko S and White R D 2015 *Phys. Rev. A* **91** 052710
- [90] Hernández-Ávila J L, Basurto E and de Urquijo J 2002 *J. Phys. D: Appl. Phys.* **35** 2264
- [91] Basurto E, Hernández-Ávila J L, Juárez A M and de Urquijo J 2013 *J. Phys. D: Appl. Phys.* **46** 355207
- [92] de Urquijo J, Mitrani A, Ruíz-Vargas G and Basurto E 2011 *J. Phys. D: Appl. Phys.* **44** 342001
- [93] Bekstein A, de Urquijo J, Ducasse O, Rodríguez-Luna J C and Juárez A M 2012 *J. Phys.: Conf. Ser.* **370** 012006
- [94] Cheung B and Elford M T 1990 *Aust. J. Phys.* **43** 755
- [95] Band R, Petrović Z L and Crompton R W 1987 *Aust. J. Phys.* **40** 347
- [96] Dupljanin S, de Urquijo J, Šašić O, Basurto E, Juárez A M, Hernández-Ávila J L, Dujko S, Petrović Z L and Jovanović J 2010 *Plasma Sources Sci. Technol.* **19** 025005
- [97] Šašić O, Dupljanin S, Urquijo J D and Petrović Z L 2013 *J. Phys. D: Appl. Phys.* **46** 325201
- [98] Robson R E 1984 *Aust. J. Phys.* **37** 35
- [99] Petrović Z L, Crompton R W and Haddad G N 1984 *Aust. J. Phys.* **37** 23
- [100] Vrhovac S B and Petrović Z L 1996 *Phys. Rev. E* **53** 4012
- [101] Jovanović J V, Vrhovac S B and Petrović Z L 2004 *Eur. Phys. J. D* **28** 91
- [102] Šašić O, Jovanović J, Petrović Z, de Urquijo J, Castrejón-Pita J, Hernández-Ávila J and Basurto E 2005 *Phys. Rev. E* **71** 046408
- [103] Alves L L *et al* 2013 *J. Phys. D: Appl. Phys.* **46** 334002
- [104] Skullerud H R 2017 *Plasma Sources Sci. Technol.* **26** 045003
- [105] Konovalov D A, Cocks D G and White R D 2017 *Eur. Phys. J. D* **71** 258
- [106] Dujko S, Raspopović Z M, White R D, Makabe T and Petrović Z L 2014 *Eur. Phys. J. D* **68** 166
- [107] Boyle G J, Tattersall W J, Cocks D G, McEachran R P and White R D 2017 *Plasma Sources Sci. Technol.* **26** 24007
- [108] White R D and Robson R E 2009 *Phys. Rev. Lett.* **102** 230602
- [109] White R D and Robson R E 2011 *Phys. Rev. E* **84** 031125
- [110] Van Hove L 1954 *Phys. Rev.* **95** 249
- [111] McEachran R P and Stauffer A D 1990 *J. Phys. B: At. Mol. Opt. Phys.* **23** 4605
- [112] Mimmagh D J R, McEachran R P and Stauffer A D 1993 *J. Phys. B: At. Mol. Opt. Phys.* **26** 1727
- [113] Chen S, McEachran R P and Stauffer A D 2008 *J. Phys. B: At. Mol. Opt. Phys.* **41** 25201
- [114] Buckman S J, Cooper J W, Elford M T and Inokuti M 2003 *Photon and Electron Interactions with Atoms, Molecules and Ions* ed Y Itikawa vol 17A (Darmstadt: Springer) pp 2–35
- [115] Robertson A 1977 *Aust. J. Phys.* **30** 39
- [116] Laplace database (<http://lxcat.net>) (Accessed: March 2017)
- [117] Miller L S, Howe S and Spear W E 1968 *Phys. Rev.* **166** 871
- [118] Halpern B, Lekner J, Rice S and Gomer R 1967 *Phys. Rev.* **156** 351
- [119] Dutton database (<http://lxcat.net>) (Accessed: March 2017)
- [120] Warren R W and Parker J H 1962 *Phys. Rev.* **128** 2661
- [121] Townsend J S and Bailey V A 1922 *Phil. Mag.* **44** 1033
- [122] Shibamura E, Takahashi T, Kubota S and Doke T 1979 *Phys. Rev. A* **20** 2547
- [123] Bordage M C, Biagi S F, Alves L L, Bartschat K, Chowdhury S, Pitchford L C, Hagelaar G J M, Morgan W L, Puech V and Zatsarinny O 2013 *J. Phys. D: Appl. Phys.* **46** 334003
- [124] Pack J L, Voshall R E and Phelps A V 1962 *Phys. Rev.* **127** 2084
- [125] Schnyders H, Rice S A and Meyer L 1966 *Phys. Rev.* **150** 127
- [126] Jacobsen F M, Gee N and Freeman G R 1986 *Phys. Rev. A* **34** 2329
- [127] Yoshino K, Sowada U and Schmidt W F 1976 *Phys. Rev. A* **14** 438
- [128] Reininger R, Asaf U, Steinberger I and Basak S 1983 *Phys. Rev. B* **28**
- [129] Space B, Coker D F, Liu Z H, Berne B J and Martyna G 1992 *J. Chem. Phys.* **97** 2002
- [130] Metzler R and Klafter J 2004 *J. Phys. A: Math. Gen.* **37** R161
- [131] Metzler R, Barkai E and Klafter J 1999 *Phys. Rev. Lett.* **82** 3563
- [132] Scher H and Montroll E 1975 *Phys. Rev. B* **12** 2455
- [133] Stokes P W, Philippa B, Read W and White R D 2015 *J. Comput. Phys.* **282** 334
- [134] Cocks D G and White R D Fluctuation capture in non-polar gases and liquids arXiv:1602.07834